2007 Geophysical Surveys of the Birds Hill Esker-Delta Complex at Birds Hill Provincial Park, Manitoba

T. Unrau, C. Tycholiz, I. Ferguson, A. Frederiksen, M. Serzu

Dept. of Geological Sciences
University of Manitoba
Winnipeg Manitoba, R3T 2N2

August 2008

Contact Address:
Ian Ferguson, Prof.
Department of Geological Sciences
University of Manitoba
Winnipeg, MB, Canada, R3T 2N2
Phone: (204) 474-9154, Fax (204) 474-7623
E-mail: ij_ferguson@umanitoba.ca

2007 Geophysical Surveys of the Birds Hill Esker-Delta Complex at Birds Hill Provincial Park, Manitoba

T. Unrau, C. Tycholiz, I. J. Ferguson, A. Frederksen, M. Serzu

Dept. of Geological Sciences
University of Manitoba
Winnipeg Manitoba, R3T 2N2

Summary

As part of the University of Manitoba, Department of Geological Sciences, Geophysics Field School for 2007, geophysical surveys were performed at Birds Hill Park, Manitoba. The geological setting includes glaciolacustrine and other glacial sediments. Measurements were made at two sites: Site 1 is near the Overlook on North Drive and has UTM coordinates 651980E 5542980N (Zone 14, NAD83) and Site 2 is south of West Shore Road adjacent to the Parking Lot and with UTM coordinates 651330E 5542780N. Geophysical methods used were DC-resistivity, terrain conductivity, time domain electromagnetics (TEM), and seismic refraction. These geophysical data were analyzed and interpreted using standard methods and results from previous studies at the sites were integrated into the interpretation.

At Site 1 the upper few metres of the surficial sediments, corresponding to a littoral sand unit with high radar reflectivity, is very resistive. A rise in conductivity is observed in the southern part of the site, down the hill from the Overlook, and is interpreted to be due to an increase in either the clay content or the saturation of the geological unit beneath the littoral sands. DC-resistivity data and seismic refraction surveys were able to detect the presence of a frozen soil layer in late April 2007 between 30 and 90 cm depth. The seismic refraction and TEM results resolved deeper structures at the site. They showed that the upper surface of clay-rich basinal sediments is at a depth of around 20 m. The TEM models also showed a layer of increased conductivity at around 50 m depth but additional studies are required to confirm this result.

At Site 2 terrain conductivity results defined a linear northeast-southwest trending conductivity high that had been delineated in previous surveys at the site. The high is interpreted to be caused by an increase in the clay content of a layer extending from around 15 cm to 2-3 m depth. This layer is underlain by clay-rich basinal sediments with relatively high seismic velocity and conductivity.

Table of Contents

List of Figures

List of Tables

1. INTRODUCTION

In April and May of 2007, staff and students from the University of Manitoba completed a number of geophysical surveys in Birds Hill Provincial Park, Manitoba. The principal goal of the surveys was to familiarize students with geophysical survey techniques and equipment as part of the University of Manitoba, Department of Geological Sciences, Geophysics Field School. Additionally, the data that were collected from this survey are useful for continued investigations of the subsurface features associated with the Birds Hill esker-delta complex (Matile 1984) and can be used to support or improve geological interpretations of the existing data. The methods used to collect the new geophysical data are DC-resistivity, terrain conductivity, time domain electromagnetics (TEM), and seismic refraction.

The two sites covered in this report were previously surveyed by the Geophysics Field School in previous years. A report covering the targeted areas and their results was produced by Gowan & Ferguson (2005). Information from that report is used in the interpretation of the new data collected for this new report.

2. SURVEY AREA

Birds Hill Park is a provincial park and wildlife refuge located 24 km northeast of Winnipeg, Manitoba on provincial highway 59. Birds Hill is a Quaternary esker-glaciolacustrine complex that formed 11,000 to 12,000 years ago from the interaction of the Red River glacial ice lobe and glacial Lake Agassiz (Matile 1984).The geology is described in more detail in Gowan & Ferguson (2005).

Figure 1 shows the site locations for the current surveys. Site 1 (in blue) is just south of North Drive, and corresponds to the previously surveyed locations near the parking lot and lookout point. Site 2 (in red) is located to the south of West Shore Road and is east of the parking lot in a grassy field. The site numbers correspond to those used in previous reports.

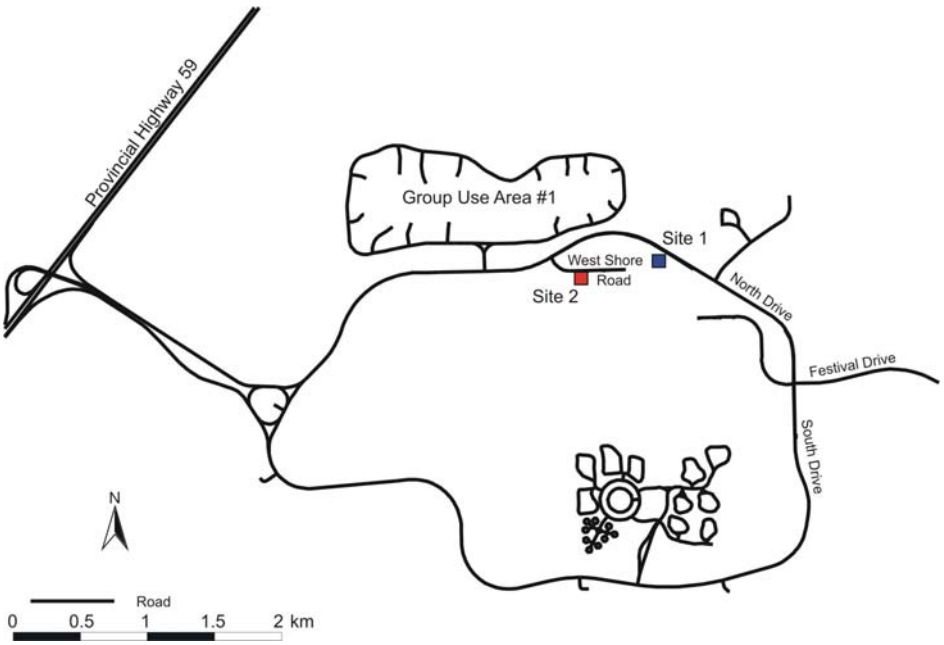

Figure 1: General map of Birds Hill Park showing the location of the 2007 geophysical surveys.

3. GEOPHYSICAL SURVEYS

3.1 Overview

The geophysical surveys were conducted at two sites using multiple methods. At Site 1, data were collected using DC-resistivity, terrain conductivity, TEM, and seismic refraction surveys (Fig. 2). At Site 2, data were collected for terrain conductivity and seismic refraction only (Fig. 3).

At Site 1 measurements were made along and adjacent to a 350 m long line running in a north-south direction (Fig. 2). The north end of this line is located at approximately 651982E 5542977N (+/- 5.0m, Zone 14, NAD83), and the site coordinates a numbered upward from 0 m toward the south end of the line. The terrain conductivity and seismic refraction profiles shared a common northern point but has slightly different azimuths with the terrain conductivity profile running geographic north-south and the seismic profile running magnetic north-south. At Site 2 a 50 m by 50 m north-south by east-west grid was constructed with a GPS measurement of its south-west corner being 651330E 5542780N (Zone 14, NAD 83). Survey lines ran east-west and were 10m apart. Seismic refraction data were collected on a north-south profile to the south of the grid (Fig. 3). The line starts at 651350E 5542670N (Zone 14, NAD 83) and is numbered with coordinates increasing to north from 0 m.

The main field school surveys took place between April 24th and April 26th 2007. The field work was done soon after spring melt had completed and there had been minimal precipitation over the last month. The soil still felt cold to the touch. Supplementary terrain conductivity measurements were made on May 18th when an EM34 terrain conductivity meter and terrain conductivity meter data logger had become available.

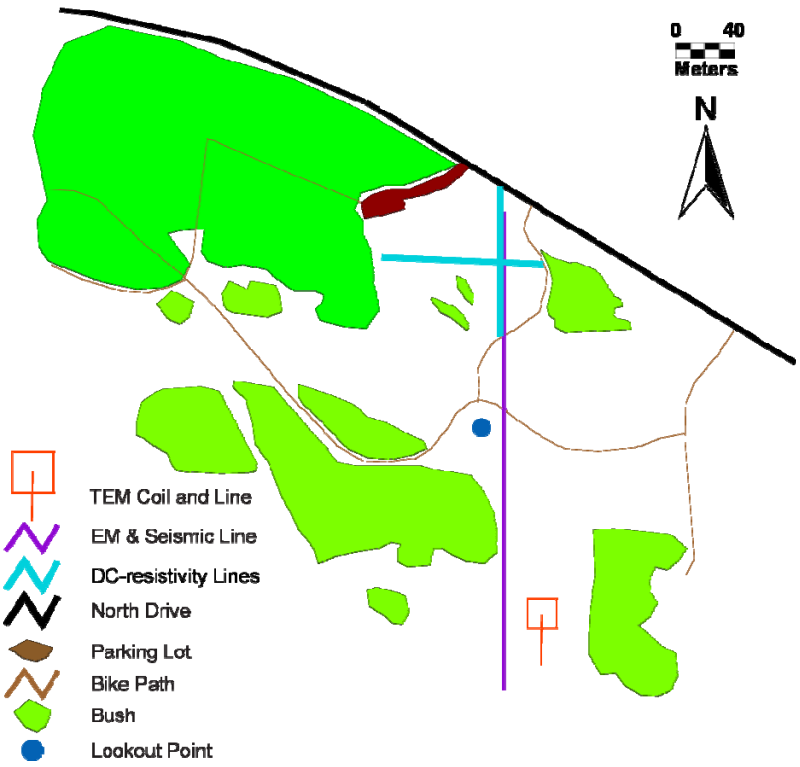

Figure 2: Map of Site 1 showing the location of geophysical surveys and major features.

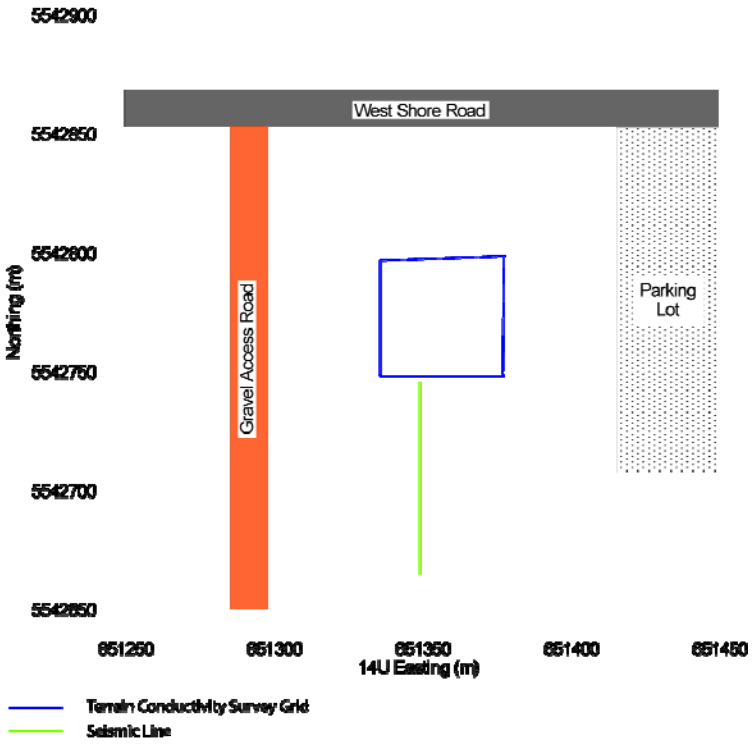

Figure 3: Map of Site 2 showing the location of geophysical surveys and major features.

3.2 Terrain conductivity

Measurements of terrain conductivity were taken at both sites in order to map lateral changes in the shallow conductivity structure. Terrain conductivity instruments transmit an inducing eddy current into the ground using a loop, which generates secondary fields that under appropriate conditions are proportional to the conductivity of the subsurface (Geonics 1991). For this survey, three different Geonics instruments were used: the EM38 which has a 1m coil separation (Fig. 4); the EM31 which has a 3.66m coil separation (Fig. 5); and the EM34-3, which has variable 10, 20 and 40m coil separations (Fig. 6).

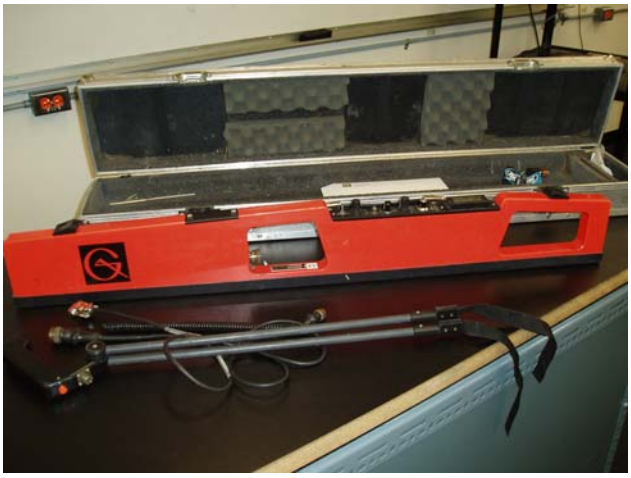

Figure 4: Picture of a Geonics EM38 (photograph by P. Bucher).

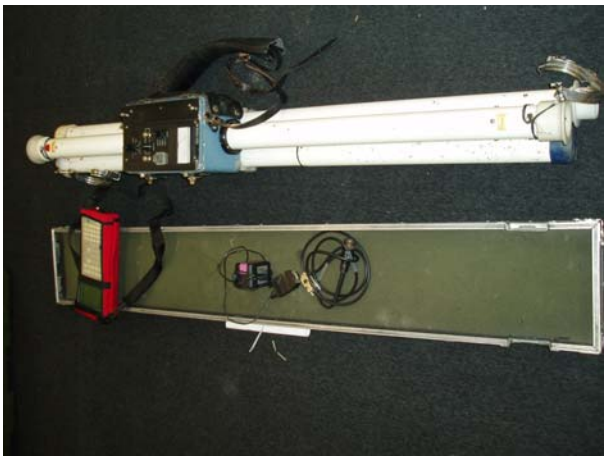

Figure 5: Picture of an Geonics EM31 (photograph by P. Bucher).

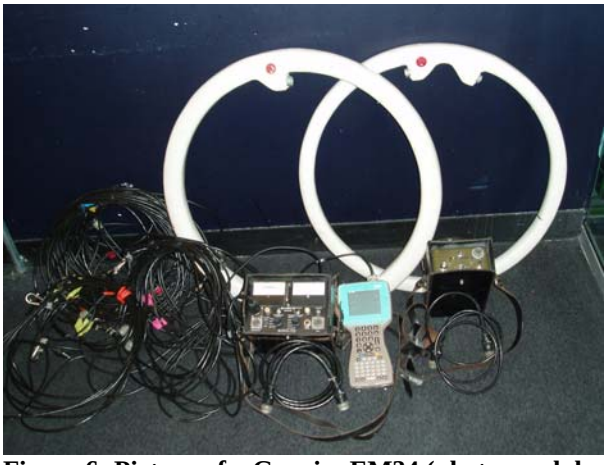

Figure 6: Picture of a Geonics EM34 (photograph by P. Bucher).

Terrain conductivity instruments can be operated in four different orientations. Each instrument can be positioned such that the coils are producing a field in the vertical or horizontal direction. The two dipole modes yield a different depth of signal penetration, and are useful in gauging the conductivity variation with depth. Additionally, the instruments can be oriented parallel or perpendicular to the line direction. The parallel and perpendicular responses are similar except when crossing over linear features, such as pipes, in which case the instruments will produce a very strong or very weak response depending on the orientation relative to the pipe. The terrain conductivity is determined from the measured quadrature (90^o out of phase) response. With a data logger attached, the EM38 and EM31 can simultaneously record the in-phase response which is sensitive to magnetic and extremely conductive bodies.

The penetration depths for the terrain conductivity instruments depend on the operating frequency, coil separation, and orientation (Geonics 1991). However, in many settings the recorded apparent conductivities can be estimated to correspond to depths of 0.375 times the coil separation for horizontal orientations, and 0.866 times the coil separation for vertical modes. These are the depths above and below which material contributes 50% of the response. For the EM38, the penetration depths are 37.5 cm for horizontal mode, and 86.6 cm for vertical mode.. The EM31 measures 1.37 m in horizontal mode, and 3.17 m in vertical mode, making it complementary to a long soil auger in soil analysis. The EM34 can measure six depths ranging

from 3.75 m to nearly 35 m providing information on the deeper subsurface. Using multiple coil separations one can assemble a pseudosection of the conductivity by plotting recorded values at the corresponding penetration depth.

Measurements of terrain conductivity were made along the main profile line at Site 1 (Fig. 2). EM31 and EM38 measurements were taken with the instrument perpendicular to the line and EM34 measurements with the instrument parallel to the line.

- EM38 measurements were made using a 2 m spacing along the northern 50 m of this line in both horizontal and vertical mode on April 24th. A data logger was not used and only the quadrature response was recorded.
- EM31 measurements were made using a 5 m spacing along the northern 250 m of the line in both horizontal and vertical mode on April 24th. A data logger was not used and only the quadrature response was recorded.
- Additional EM31 measurements were made on May 28th along the whole line at 5 m spacing using a data logger. Vertical and horizontal mode in-phase and quadrature responses were recorded.
- EM34 measurements were made using 10 m and 20 m coil spacings along the whole line on May 28th.

At Site 2 terrain conductivity recordings were made on April 24th on the 50 m by 50 m grid. Due to time constraints, measurements were not done on the 50 N line. The orientation of the instrument relative to the line direction was not recorded.

- EM38 measurements were made using a 1 m station spacing in both horizontal and vertical modes along lines 20N and 30N. A data logger was not used and only the quadrature response was recorded
- Vertical dipole EM31 measurements were made using a 5 m spacing on lines 0N, 10N, 20N, 30N and 40N and horizontal dipole measurements were made on lines 0 N and 10 N. A data logger was not used and only the quadrature response was recorded.

3.3 DC-resistivity

DC-resistivity equipment measures the ground's resistivity by injecting a current into the ground using two electrodes, and measuring the voltage between two receiver electrodes located in between the two current transmitter electrodes (Bison Instruments 1975). Depth of penetration increases as the spacing between the electrodes is increased. DC-resistivity measurements were collected using a Earth Resistivity Meter Model 2350 by Bison Instruments (figure 7). Measurements were made using a Wenner array in which the spacing between the four electrodes is equal. This array optimizes the vertical resolution and the ability to detect lateral inhomogeneities (Reynolds, 1997).

Orthogonal DC soundings were recorded at Site 1 on April 26th. The first sounding was aligned along the terrain conductivity profile, with the midpoint of the array corresponding to the 57 m mark on that line. The electrode spacing for this sounding ranged from 0.1 m to 40 m and was limited by the road. The midpoint of the sounding was recorded by GPS as 651979E, 5542933N (Zone 14, NAD83). The second sounding was oriented perpendicular to the first line, but shifted around 35 m to the west in order to allow for a longer line. The position of the midpoint was recorded by GPS as 651945E 5542932N (Zone 14, NAD83) and the line azimuth was recorded as 98°. The electrode spacing for this line ranged from 0.2m to 45m and was limited by the location of trees.

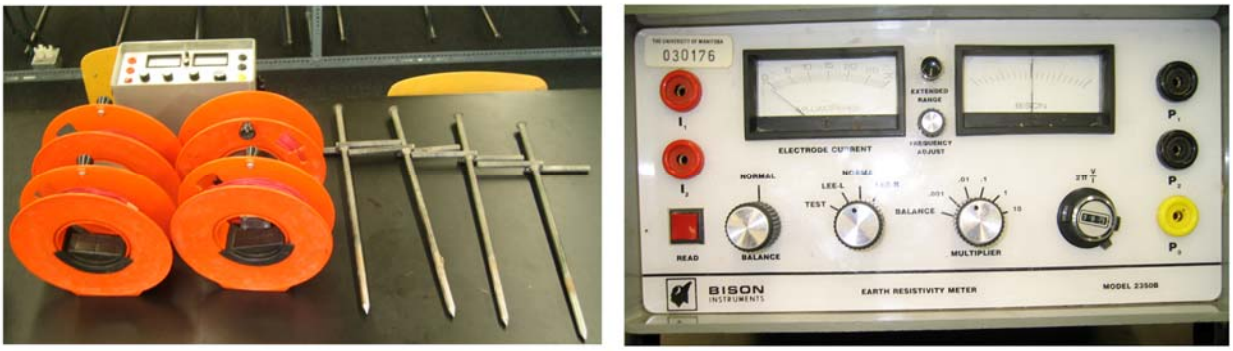

Figure 7. Picture of BISON Earth Resistivity Meter and associated equipment.

3.4 Time domain electromagnetics

TEM measures the conductivity structure of the deeper earth. In the method a current in a large transmitter loop is shut off very rapidly. This change induces a current ring in the Earth beneath the loop that subsequently diffuses outwards and downwards. This current can best be visualized as a 'smoke ring' expanding into the Earth. The strength of the current increases with increasing conductivity of the Earth and the rate of outwards diffusion decreases. The decaying current creates a secondary magnetic field that is measured in a series of time-gates by a receiver coil (Reynolds 1997). As the signal propagates outwards, it reaches deeper layers, which are therefore observed at later times in the recorded data. The signals decay approximately exponentially, so the intervals in which the instrument takes measurements are selected so as to become progressively longer in order to reflect the decay rate. Multiple recordings are taken wherever possible in order to reduce the interference from noise.

Figure 8 shows the general configuration of a TEM sounding. The receiver coil can be positioned outside the transmitter loop as shown or in the centre of the loop. The 2007 TEM soundings were done using a Geonics PROTEM47 system which measured in relatively short-time time gates and is suitable for near-surface studies. Figure 9 shows a photograph of the equipment.

A data conversion program converts the instrument readings, which are in volts, into estimates of apparent resistivity or its inverse, apparent conductivity. This conversion is often a late-time estimate which assumes that the signal propagation distance exceeds both the transmitter loop dimensions and the distance from the loop to the receiver.

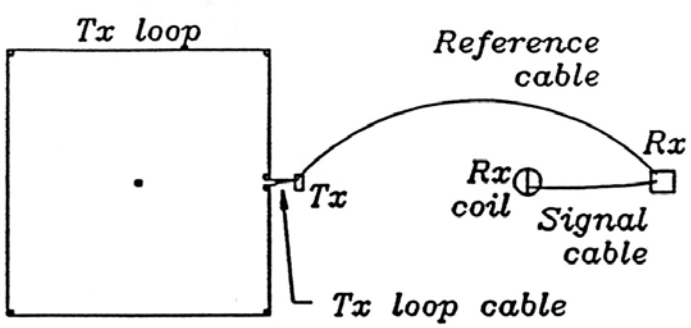

Figure 8: General configuration of TEM system.

Figure 9: Picture of Geonics PROTEM 47 (photograph by P. Bucher).

A TEM sounding was taken at Site 1 (Fig. 2) on April 26th. The sounding used a 20m by 20m square loop, with the receiver operating at distances along a line extending southwards from the centre of the loop. Measurements were made at UH and VH frequencies. These settings provide PROTEM47 readings at early and intermediate time-gates.

3.5 Seismic refraction

Seismic refraction surveys determine the seismic velocity structure of the Earth. Measurements are made at a series of offsets from a source and analysis focuses on detections of seismic signals that have been refracted along subsurface layers (Reynolds 1997). Such signals are usually observed in structures in which the seismic velocity increases with depth. Seismic refraction surveys were done at both sites using a Geometrics Geode ES-3000 hammer seismic system, configured for 24 channel recording.

At Site 1 seismic profiles were done on the northern part of the profile (Fig. 2) on April 24th. Five profiles were recorded at this location with some data redundancy. The configurations are recorded in Table 1 and shown in Figure 10. At Site 2, four profiles were completed along a 75 m long line (Fig. 3). The locations of the individual profiles are listed in Table 2 (Fig. 10).

Table 1: Seismic line configurations and data file names

Site	Line	Shot Location	Receiver Direction	Receiver Separation	Stacking	Datafile
1	1	0m	South	1m	4	100101.dat
1	1	0m	South	1m	4	100102.dat
1	1	0m	South	1m	4	100103.dat
1	2	0m	South	3m	4	100201.dat
1	2	0m	South	3m	9	100202.dat
1	3	75m	North	3m	9	100301.dat
1	4	52m	North	1m	4	100401.dat
1	5	27m	South	1m	4	100501.dat
2	1	0m	North	1m	4	200101.dat
2	2	0m	North	3m	4	200201.dat
2	3	75m	South	3m	4	200301.dat
2	4	75m	South	1m	4	200401.dat

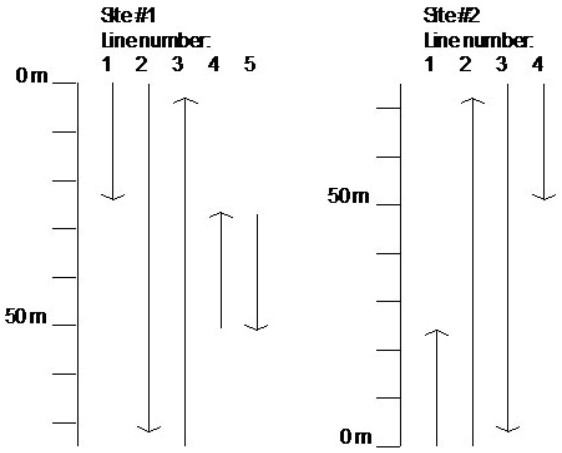

Figure 10: Seismic profile configurations. The hammer shot is at the tail end of the arrows and the specified geophone locations increase in the direction of the arrows.

At both sites, the data files were recorded using a laptop and logging software that accompanied the equipment. Between 4 and 9 hammer shots were stacked in each recording in order to increase the signal to noise level. Files were stored in SEG-2 format, using the following naming convention: A00BCC.dat, where A is the site number, B is the line number, and CC is the recording number (Table 1).

4. SITE 1: DATA ANALYSIS AND INTERPRETATION

4.1 Survey results and data analysis

4.1.1 Terrain conductivity

The terrain conductivity data are listed in Appendix A. Figure 11 shows the EM38 results. The responses show a sharp anomaly at 24 to 26 m where there is a positive horizontal dipole-mode response and a negative vertical dipole-mode response. Such responses are characteristic of a buried linear conductor, such as an electrical cable. For the rest of the profile the apparent conductivity values are less than 10 $mS.m^{-1}$. For the northern 35 m of the profile the horizontal readings is in the range 3 to 7 $mS.m^{-1}$ and the vertical dipole reading are <2 $mS.m^{-1}$. The results indicate that the conductivity is decreasing with depth in the shallow (<1 m depth) subsurface. South of the 35 m point the horizontal reading is approximately zero and the vertical dipole reading is in the range 2 to 8 $mS.m^{-1}$ and the results indicate that the conductivity is decreasing with depth.

The EM31 responses are plotted together on a single profile, along with the EM34 response, since they cover roughly the same region, and show the same trends (Fig. 12). All of the responses show an increase in apparent conductivity with distance south along the profile. As observed in the EM38 data the apparent conductivity is very low for the first 50 m of the profile. It then increases in an approximately linear manner from around the 100 m point to the 350 m point. The EM34 responses are more conductive than the EM31 responses indicating an increase in conductivity with depth. Finally, the EM31 and EM34 data show a number of localized anomalies consistent with the profile crossing linear features. Strong anomalies are observed at 185 m in the EM31 data at an observed water pipe and at 200 and 350 m in the EM34 data.

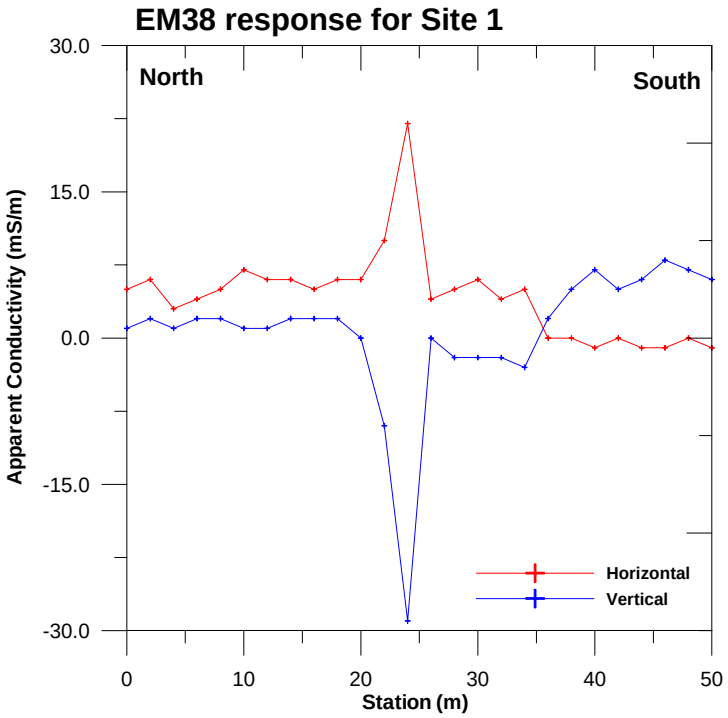

Figure 11: EM38 apparent conductivity response for Site 1. Crosses show measurement locations.

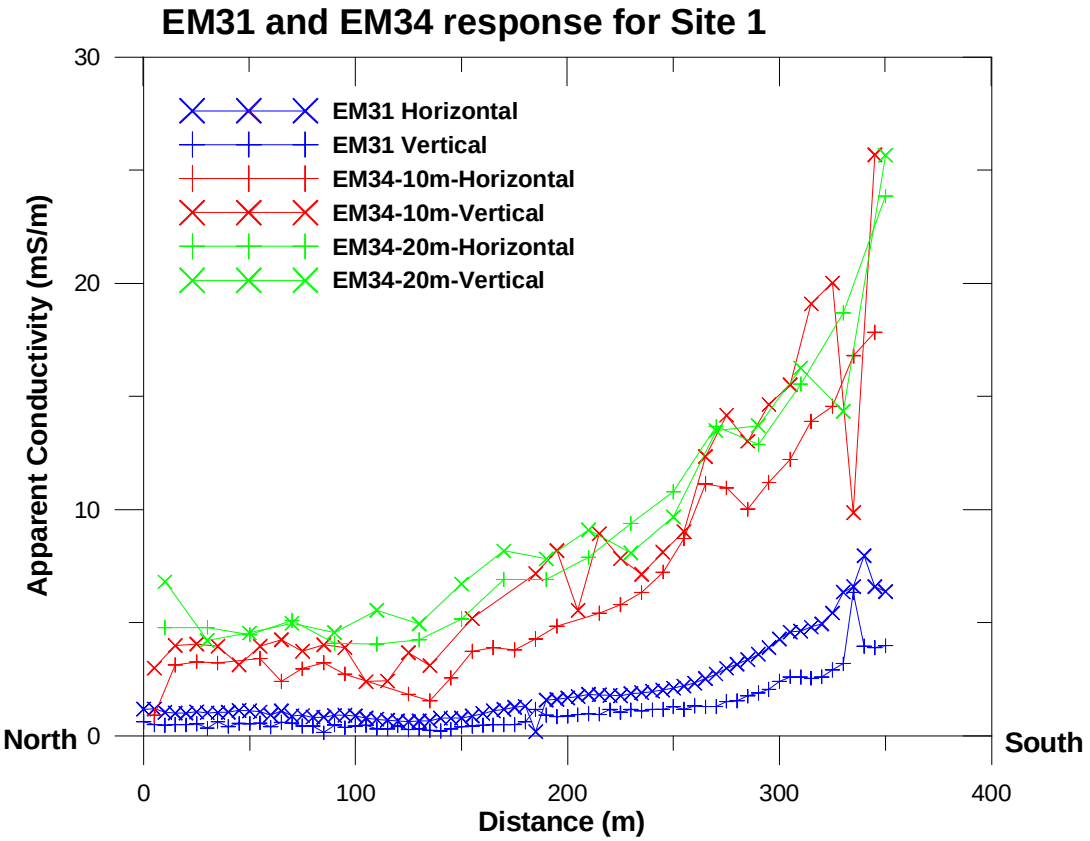

Figure 12: Apparent conductivity responses for EM31 and EM34 data for the profile at Site 1.

The data from the EM38, EM31 and EM34-3 profile can be used to produce a 2D pseudosection of the profile by assuming a reasonable estimate for the depth of penetration of each response, e.g. the depth above and below which material contributes half of the response. The pseudosection is a smoothed image of the underlying structure that provides an indication of the general shape of structures in the subsurface. Figure 10 shows the pseudosection for Site 1. The depth of each EM response was corrected for elevation using the elevation data from Gowan & Ferguson (2005) and the data then were gridded using an exponential variogram with a scale of 15 and distance of 4 m.

The pseudosection shows that at the north end of the profile the near-surface conductivity is <3 mS.m^{-1} and at greater depth the conductivity increases to around 6 mS.m^{-1}. At the south end of the line a thin (< 2 m) resistive surface layer overlies a zone with conductivity of around 10 mS.m^{-1}. The conductor observed at depth at the very south end of the line is interpreted to be a man-made object since as shown in Figure 9 it causes positive and negative anomalies on different measured responses.

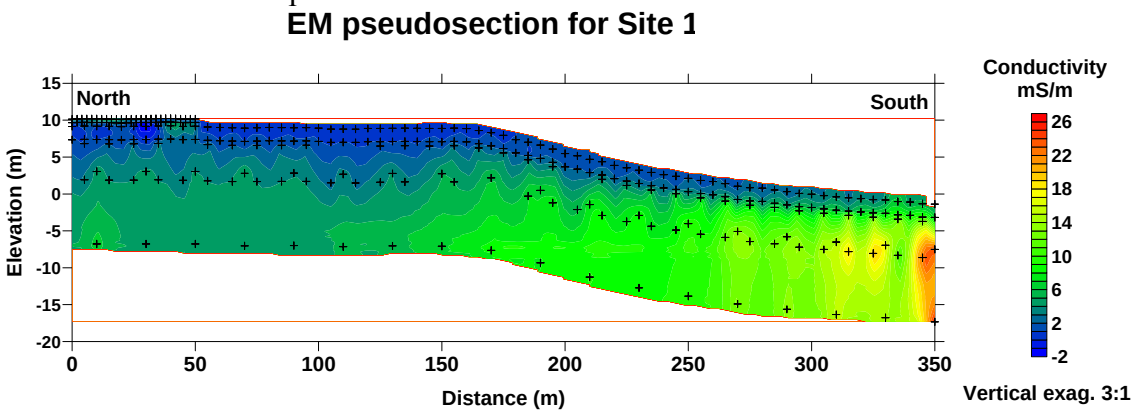

Figure 13: Terrain conductivity pseudosection based on EM38, EM31 and EM34-3 data for Site 1. Results have been corrected for elevation (with zero elevation corresponding to the ground surface at the south end of the profile).

4.1.2 DC-resistivity

The raw DC resistivity data are listed in Appendix B. The values of the repeated readings at each electrode spacing were averaged and the results are shown in Figure 14. The results for the two orthogonal profiles show a similar three-layer structure. There is an upper layer with a resistivity of around 200 ohm.m (5 mS.m^{-1}) overlying a layer of resistivity of >2000 ohm.m (<0.5 mS.m-1) overlying a layer with resistivity of <200 ohm.m (>5 mS.m^{-1}). The central point of the north-south profile was offset from that of the east-west profile by around 35 m and the different responses for the two profiles provides an indication of the lateral variation in the shallow resistivity structure.

The DC-resistivity data were inverted using the computer program EINVRT4 (Sandberg 1988). The data were converted from Wenner-array format into an equivalent Schlumberger-array format as required for input to EINVRT4 using the FORTRAN program FORCVT2. They were then inverted using three-layer models and unconstrained inversions in which all of the model parameters were allowed to vary. The resulting inversion models for the two profiles had similar thicknesses for the layers and a similar resistivity for the top layer. The inversions were then repeated with the thicknesses of the layers and the resistivity of the top layer constrained to the mean value for the unconstrained models. The results of the constrained inversions and the fit of the model responses to the data are shown in Figure 15.

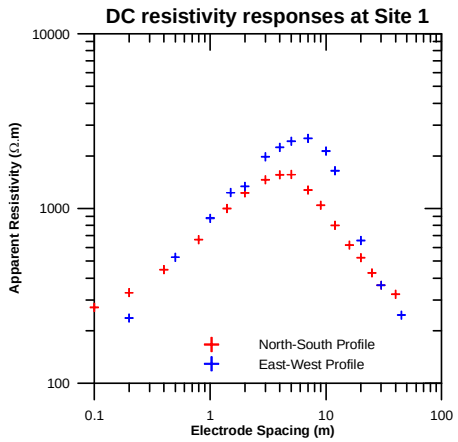

Figure 14: DC-resistivity responses at Site 1.

The final models provide a good fit to both data sets. They include an upper layer with a thickness of 28 cm and a resistivity of 220 ohm.m (4.5 $mS.m^{-1}$) and a second layer of thickness 64 cm. The second layer is very resistive and has a resistivity of >10,000 ohm.m (<0.1 $mS.m^{-1}$) on both profiles. The lower layer has a resistivity of 240 ohm.m (4 $mS.m^{-1}$) on the east-west profile and 380 ohm.m (3 $mS.m^{-1}$) on the north-south profile. The strong resistivity contrasts in the models means that the depth of penetration of the soundings is very limited with the response at electrode spacings of >50 m still exhibiting an influence from the shallow resistive layer between about 30 cm and 90 cm depth.

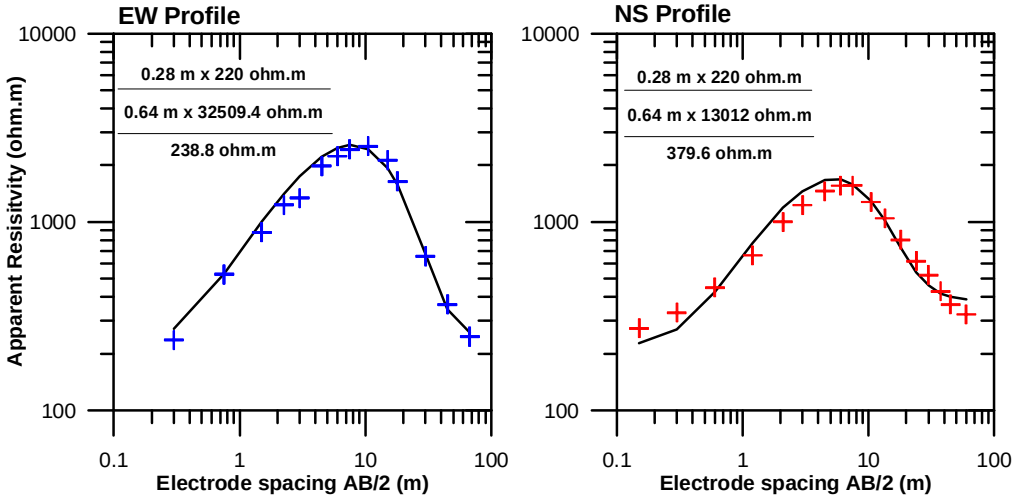

Figure 15: Three layer DC-resistivity models for Site 1. Electrode spacing is Schlumberger AB/2 value.

4.1.3 Seismic refraction

The seismic refraction data are included in Appendix C. Figure 16 shows the reversed seismic refraction data with 1 m geophone spacing from the middle of the 75 m long seismic profile. There are a number of clear arrivals and the corresponding intercepts and velocities are listed in Table 2. There is strong evidence for the direct arrival (black line) and first refraction (red line) but because these arrivals are observed on only a small number of traces the determined intercept and velocity have relatively low accuracy. The second refraction (red line) is a weak arrival with smaller magnitude than a response with the same velocity occurring about

10 ms later. Note that there is a second, faster direct arrival (green line) seen in the forward sounding and also in some places elsewhere along the profile. Most of the arrivals could be picked most accurately following reversal of the polarity of the recorded data. A weak air-wave is visible in the unreversed data.

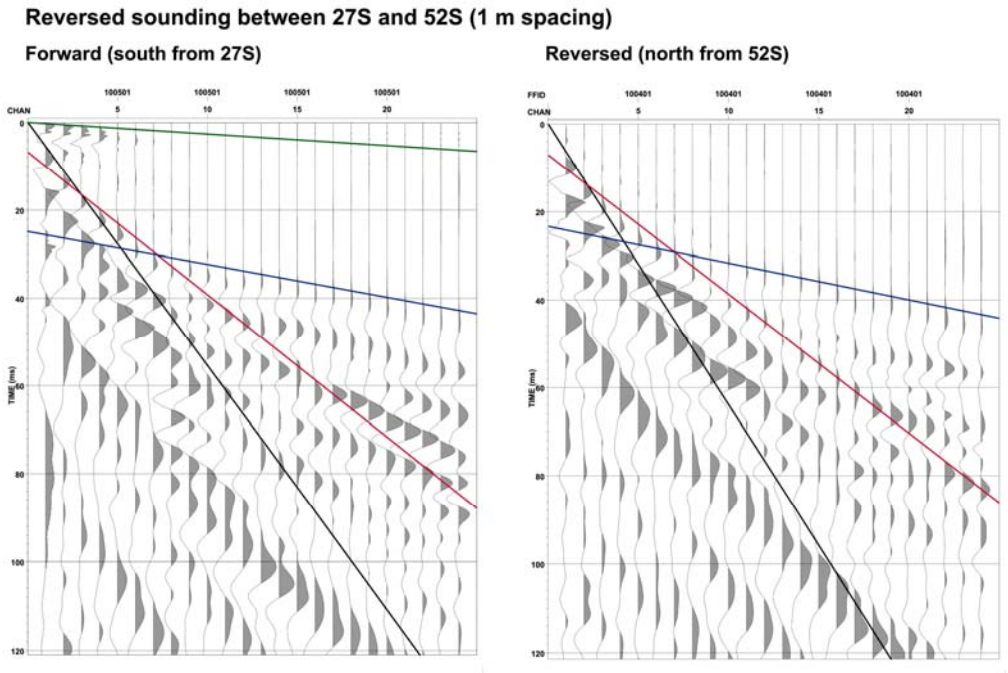

Figure 16: Forward and reverse seismic refraction data for 1 m geophone spacing and spreads at the middle of the seismic profile at Site 1.

Table 2. Arrivals fitted to Site 1 seismic refraction data.

Arrival	Intercept (ms)	Velocity (m/s)	Arrival	Intercept (ms)	Velocity (m/s)
1 m spacing data					
Forward profile. Direction: S. 100501			Reverse profile. Direction: N. 100401		
1	0	157.2/3333	1	0	180.3
2	7.18	316.4	2	7.07	307.82
3	23.57	1241.1	3	25.18	1368.63
3 m spacing data					
Forward profile. Direction: S. 100202			Reverse profile. Direction: N. 100301		
3	16.0	1144.8	3	26.0	1392.0
4	49.16	2432.1	4	46.1	2212.4

Figure 17 shows the forward and reverse soundings obtained with a 3 m geophone spacing from either end of the 75 m profile. The intercepts and slope of the two refraction arrivals picked are listed in Table 2. The first refraction picked (blue line) is a weak refraction that has a similar intercept and velocity to the second refraction noted in the 1 m geophone spacing data (Fig. 16). The second refraction (red line) does not occur as a first arrival in the 75 m spread but can be discerned as a clear second arrival at geophones located at a distance of more than 30 m form the source in both the forward and reverse profiles.

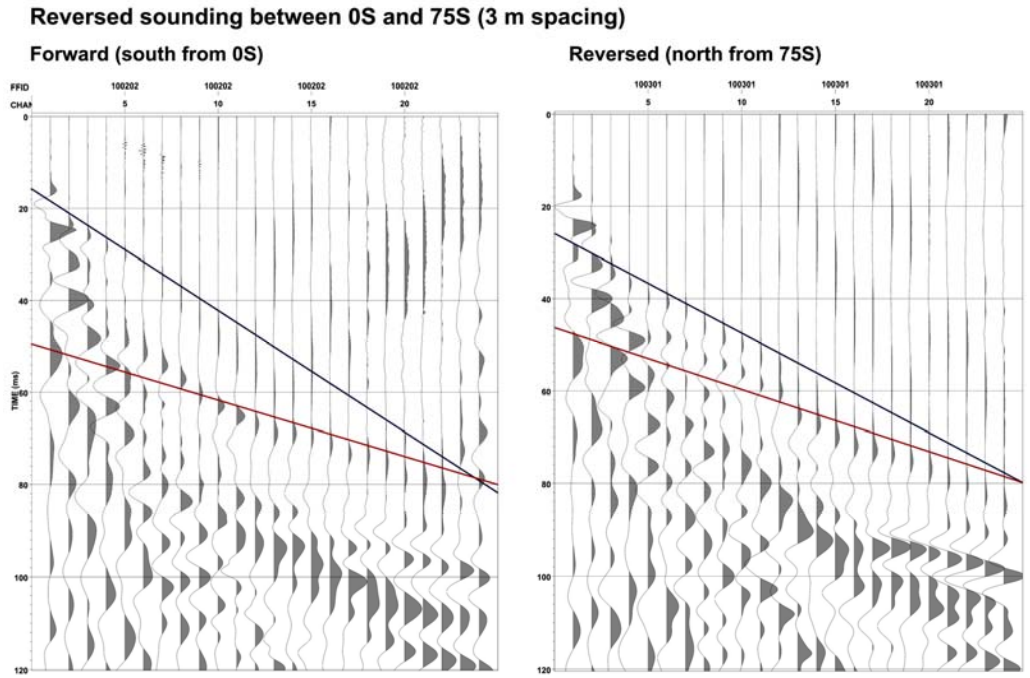

Figure 17: Forward and reverse seismic refraction shots for 3 m geophone spacing and spreads at the ends of the seismic profile at Site 1.

The high velocity (3333 $m.s^{-1}$) near-surface layer at Birds Hill is interpreted to correspond to a discontinuous frozen or partially frozen layer (an interpretation supported by the presence of the resistive second layer in the DC resistivity models). According to basic seismic refraction theory, in a layered medium it not possible to observe slower refraction arrivals from layers present beneath a high-velocity surface layer. However, this theory assumes that the seismic wavelengths are relatively small compared with the layer thickness. At Birds Hill Site 1 the velocity in the surface layer is 3333 $m.s^{-1}$ and the period of the arrivals ranges from approximately 1 ms to >10 ms suggesting wavelengths in the frozen layer of around 3 to >30 m. Assuming that the thickness of the layer is significantly less than the longest wavelengths it will be possible for lower frequency energy to "leak" from the bottom of the frozen layer and to create the slower refraction arrivals. The observation of relatively short period signals in the fast arrival that are absent in the later arrivals (Figure 16) supports this hypothesis. In this situation it appears reasonable to interpret the later refractions using classic layered-medium refraction theory.

Table 3 lists the seismic model fitted to each of the shots shown in Figures 16 and 17 using theory appropriate for a locally horizontally-layered medium (e.g., Telford et al. 1991). The interpretation was first done for the 1 m geophone spacing profile and shows quite good agreement of interface depths in the forward and reverse directions. There is an interface at around 0.75 m depth and one at around 3.3 m depth. The results provide some evidence that the lower interface is dipping. The higher velocities and intercept time for the corresponding refraction are observed to be higher for the northward sounding (at the south end) indicating that the northward direction is the up-dip direction. This interpretation is consistent with the calculation of a deeper interface at the south end of the profile. Assuming the first interface is horizontal the standard formula (Telford et al. 1991) indicates a dip angle of 0.7^{o} for the second interface.

Table 3. Models fitted to Site 1 seismic refraction data.

Layer	Velocity (m/s)	Thickness (m)	Layer	Velocity (m/s)	Thickness (m)
1 m spacing data					
Forward profile. End: north. File 100501			Reverse profile. End: south. File 100401		
1	157.2	0.65	1	180.3	0.79
2	316.4	2.51	2	307.82	2.61
3	1241.1		3	1368.63	
3 m spacing data					
Forward profile. End: north. File 100202			Reverse profile. End: south. File 100301		
2	(316.4)	1.285	2	(307.82)	2.975
3	1144.8	21.31	3	1392.0	17.71
4	2432.1		4	2212.4	

The 3 m geophone data were next analyzed using the assumption that the upper layer at either end of the profile was the same as in the middle of the profile and that the velocity of the second layer was the same. Table 3 lists the parameters of the second to fourth layers calculated assuming a locally horizontally-layered medium at either of the profile. The results show that the second layer is significantly thicker at the south end (consistent with the earlier interpretation of dip). This layer is underlain by a layer of approximately 20 m thickness with a lowest layer with a relatively high velocity occurring at an interface depth of around 22.5 m. The dip at the base of the second layer is calculated from the apparent velocities of the third layer to be 1.42^{o} over the length of the profile.

4.1.4 Time domain electromagnetics

The raw TEM data are listed in Appendix D. The TEM central loop response is shown in Figure 18 in terms of the measured voltage and the equivalent late-time apparent conductivity. The response is significantly higher than the noise level over the UH time range and for most of the VH time range. The apparent conductivity response shows an increase in conductivity with increasing time from a value of 8 mS.m^{-1} at the shortest UH time gates to 120 mS.m^{-1} at the longest VH time gates. The depth of penetration of the TEM response exceeds that of the terrain conductivity and DC resistivity surveys. The time-domain electromagnetic skin depth δ provides an estimate of the penetration. It is defined in metres for a non-magnetic material by:

$$\delta = \sqrt{\frac{2t}{\mu_0 \sigma}}$$

where t is the time in seconds, σ is the conductivity in S.m^{-1}, and μ_0=1.25664x10^{-6} H.m^{-1} is the absolute magnetic permeability. For a conductivity of 10 mS.m^{-1} the first UH time gate of 6.8 μs corresponds to a skin depth of 33 m.

Figure 19 compares the TEM response for the central loop receiver and a 20 m offset receiver. The 20 m offset responses are negative up until times of 40 μs indicating that the centre of mass of the "smoke ring" of current produced by the transmitter passed the receiver at around this time. The observation of these early time effects suggests that the central loop responses may also contain some early time effects in the first time gates and therefore that the observed apparent conductivity in Figure 18 may not be representative of the true conductivity. The

responses measured at 30 m and 50 m offset were erratic probably because of a loss of power to the transmitter loop.

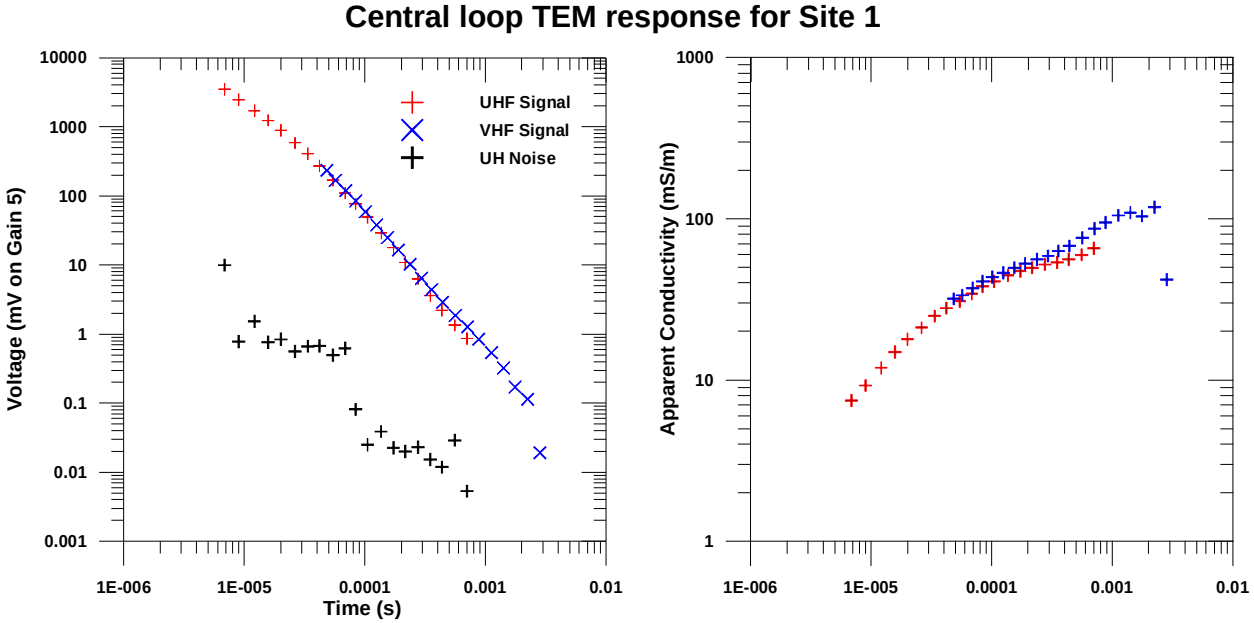

Figure 18: Central loop TEM responses at Site 1. Left panel shows the measured voltage values. Right panel shows the late-time apparent conductivity responses.

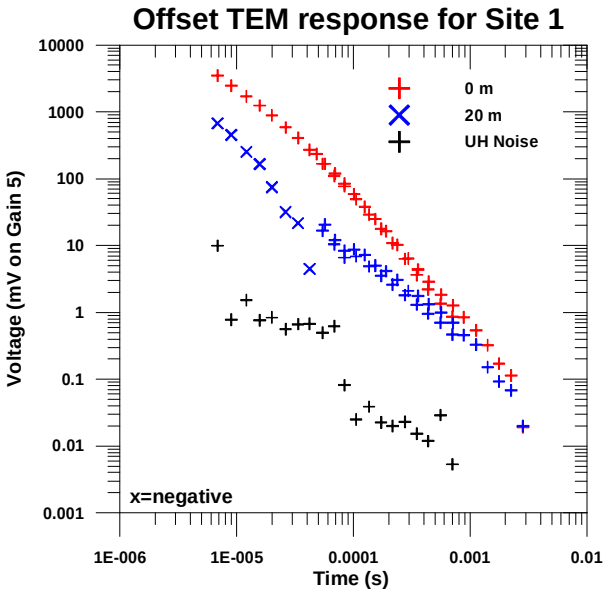

Figure 19: Offset TEM response for Site 1.

The TEM central loop responses were inverted using EINVRT4 (Sandberg 1988) and EINVRT6 (Sandberg 2005). Figure 20 shows the results. Inversions were initially done of the UH data. The data could be fitted well using a 2-layer model with an upper layer of 20 m thickness. The difference between the models for the two inversion programs suggests that the resistivity of the upper layer is not well resolved but is constrained to be <10 $mS.m^{-1}$. The resistivity of the second layer is around 100 $mS.m^{-1}$. Next the VH data were inverted using a starting model based on the UH result. The latest time data point was excluded from the

inversion. It is was not possible to fit the data satisfactorily with a two-layer model so a three-layer model was adopted. The resulting models included an upper layer of thickness of 20 m and conductivity of 6 mS.m^{-1}, overlying a middle layer of thickness of around 45 m and conductivity 110 mS.m^{-1}, and a lower layer with a poorly resolved conductivity or around 350 mS.m^{-1}. The final models for the site were obtained from joint inversion of the UH and VH data sets with the 8 latest UH time gates and the latest time VH time gate removed. The resulting three-layer models provide a good fit to the data and are quite similar to the VH inversion results (Fig. 20).

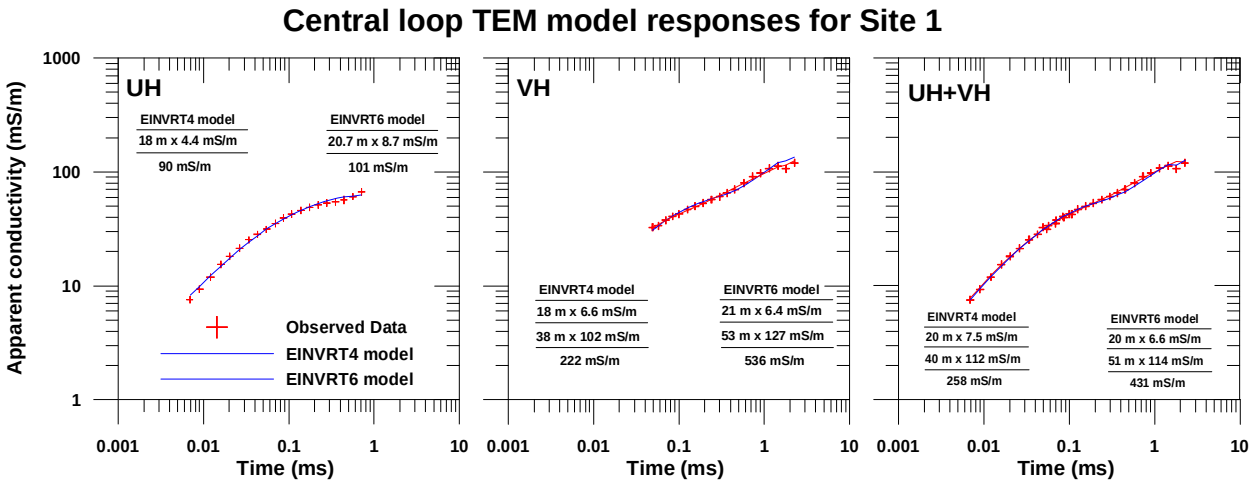

Figure 20: TEM inversion models and model responses.

4.2 Integrated data analysis and interpretation

4.2.1 Near-surface structure

The near surface structure at Site 1 can be determined from the DC-resistivity, seismic refraction, and terrain conductivity data collected at the site, as well as from GPR data collected in previous studies (Gowan & Ferguson 2005). Figure 21 shows the GPR data from Site 1 superimposed on the terrain conductivity pseudosection. There is good spatial correlation between the data sets. For example, the surface layer of strongly reflective material has a consistent conductivity of less than 3 mS.m^{-1}. At the north end of the profile this surface layer is underlain by moderately reflective material with conductivity of 5 to 10 mS.m^{-1}. At the south end of the line the conductivity of the underlying material exceeds 15 mS.m^{-1} and there appears to be minimal GPR penetration.

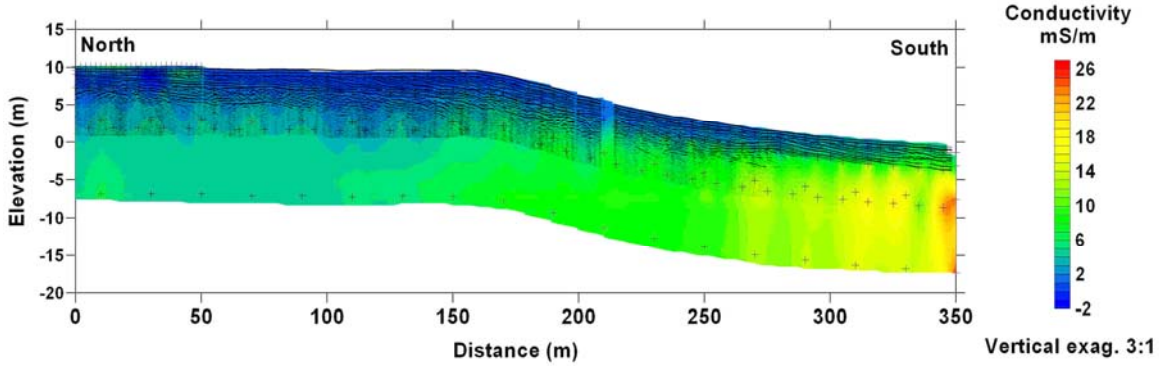

Figure 21: Terrain conductivity pseudosection overlain with GPR data from Gowan & Ferguson (2005).

Comparison of the observations with a geological cross-section (Fig. 22) indicates that the resistive, reflective unit corresponds to littoral sands. The GPR data shows that this unit is composed of south-dipping features. The seismic refraction models define a layer interface corresponding to the base of the reflective surface unit in which the seismic velocity increases from around 300 $m.s^{-1}$ to around 1200 $m.s^{-1}$. The thickness of the overlying layers is around 2 m at the north end of the seismic profile and around 4 m at the 75 m south mark.

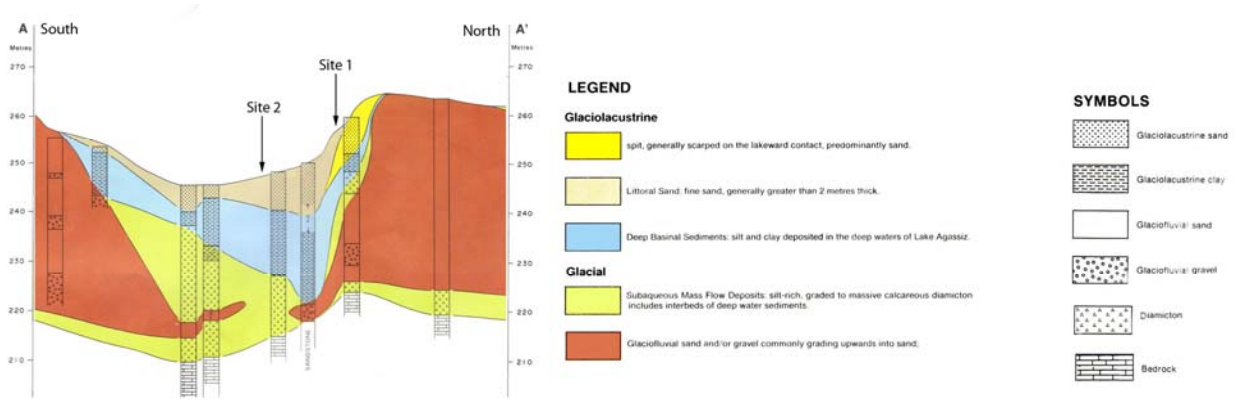

Figure 22: Approximate north-south cross-section through central parts of Birds Hill showing the general stratigraphy interpreted from drill-hole data (modified from Matile 1984). The approximate setting of the two survey sites is marked.

The nature of the material beneath the littoral sand unit is less clear. The moderate reflectivity suggests the units have a more massive nature than the littoral sands and the geological cross-section suggests the unit consists of spit deposits. The increasing conductivity of the units with distance south along the profile could be due to an increasing silt or clay content of the deposits. However, considering the elevation change along the profile the change in conductivity could alternatively be explained by increasing water content in the near-surface sediments.

A result observed in 2007 but not in previous studies at the site (Gowan & Ferguson 2005) was the observation of a shallow resistive high-velocity layer that is interpreted to be a frozen layer. Seismic refraction results suggest the layer extends from around 30 cm to 90 cm depth and has a resistivity exceeding 10,000 ohm.m. The seismic refraction data indicates a seismic velocity of ~3300 $m.s^{-1}$. The observed resistivity and velocity are consistent with the expected values for frozen sand (e.g., Scott et al. 1990). The frozen layer significantly reduces the depth of investigation of the DC resistivity data meaning that the method was unable to provide constraints on the deeper structure. In previous studies, DC-resistivity results resolved an increase in conductivity from around 1 $mS.m^{-1}$ to around 10 $mS.m^{-1}$ at 6 to 10 m depth. These results are consistent with the terrain conductivity pseudosection of the present study.

4.2.2 Deeper structure

The seismic refraction and TEM models for Site 1 indicated the presence of an interface at around 20 m depth corresponding to an increase to seismic velocities to ~2300 $m.s^{-1}$ and an increase in conductivity to ~100 $mS.m^{-1}$. This interface is interpreted to be the upper surface of the deep basinal sediments (Fig. 22). The interpreted velocity and conductivity are consistent with the presence of firmly-consolidated clay-rich material at this depth.

Based on the drilling results, bedrock is expected to occur at a depth of around 40 m beneath Site 1 (Fig. 22). The seismic refraction data did not extend to sufficient offsets to define this interface and the TEM data did not appear to resolve it. Constrained inversions indicated that it would be possible for the resistivity model to include a ~10 thick layer of conductivity of ~3 $mS.m^{-1}$ at 40 depth without changing the TEM response significantly. Therefore it would be possible for there to be a thin layer of bedrock above the basal conductive layer.

The cause of the basal layer of increased conductivity is uncertain. Magnetotelluric soundings made several kilometers to the north resolved a conductive layer at a depth of approximately 100 m interpreted to be associated with shale and/or saline brines in the Winnipeg Formation. However, constrained inversions of the TEM data indicate that the data require the conductive unit to be at a significantly more shallow depth, less than about 50 m. Additional data collection using the HI frequency mode will be necessary to fully resolve the depth of the conductor and to determine whether it represents a true layer or a two-dimensional feature that is incorrectly imaged in the one-dimensional inversions.

4.3 Conclusions

Terrain conductivity, seismic refraction, DC-resistivity and TEM surveys were completed at Site 1 to determine the geophysical characteristics of the site. The terrain conductivity results were consistent with past findings. The upper few metres of the surficial sediments, corresponding to a littoral sand unit with high radar reflectivity, is very resistive. A rise in terrain conductivity is observed in the southern part of the site and is interpreted to be due to an increase in the clay content or the saturation of the unit underlying the littoral sands. DC-resistivity data and seismic refraction were able to detect the presence of a frozen soil layer between 30 and 90 cm depth during surveys done in late-April 2007. Seismic and TEM results resolved deeper structures including the upper surface of basinal sediments at around 20 m. The source of increased conductivity at around 50 m depth in the TEM models is uncertain.

5. SITE 2: DATA ANALYSIS AND INTERPRETATION

5.1 Survey results and data analysis

5.1.1 Terrain conductivity

The raw terrain conductivity data from Site 2 are listed in Appendix 1. The EM38 responses are shown in contoured form in Figure 23. The overall pattern of the response is similar for both modes. The vertical dipole apparent conductivity tends to be higher than the horizontal dipole value indicating an increase in conductivity with depth. The apparent conductivity is highest in the southwest corner of the grid and lowest in a region around (40E,30N). The apparent conductivity values are higher than observed on the north end of site 1 and range from around 10 to 50 $mS.m^{-1}$.

The EM31 responses are also shown in Figure 23. The pattern of the response is again similar for both modes with the vertical dipole response being higher than the horizontal dipole response. The most complete data set is available for the EM31 vertical dipole mode. This mode shows that the conductivity structures are striking in a northwest-southeast direction and that there is a conductivity high crossing the southwest corner of the grid and a low crossing through the northeast corner. In this mode the high has apparent conductivity of >50 $mS.m^{-1}$ and the low has values of <30 $mS.m^{-1}$.

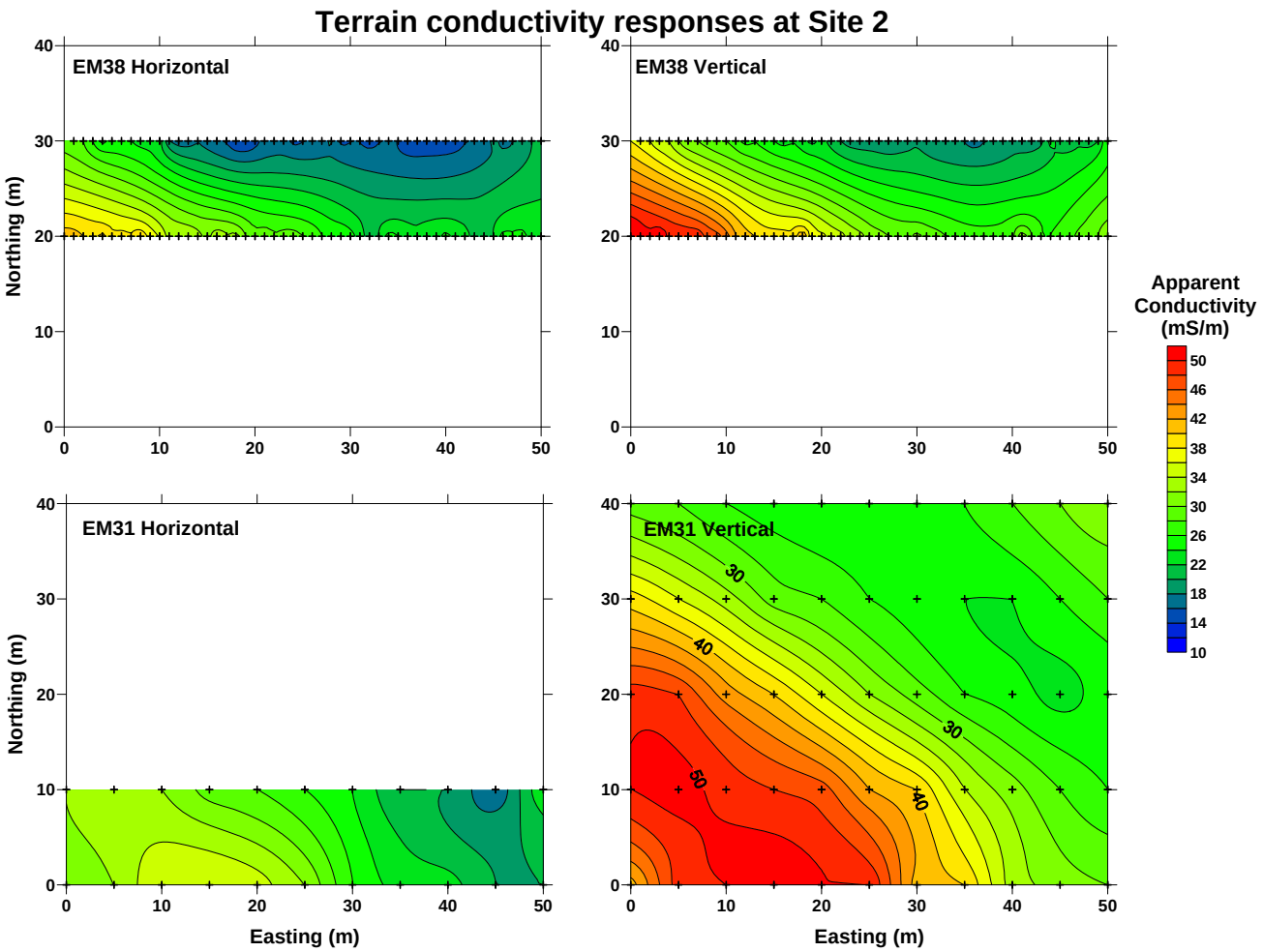

Figure 23: EM38 and EM31 apparent conductivity responses from Site 2. Measurements were not available at all points for all modes and crosses on the figures show the location of available data. Data were interpolated using default linear variogram models in Surfer 8.0.

5.1.2 Seismic refraction

The Site 2 seismic refraction data is include in Appendix C. Figure 24 and 25 show the seismic refraction data with 1 m and 3 m geophone spacing from the either end of the 75 m long seismic profile and Table 4 tabulates the parameters of the fitted arrivals. There is good evidence for the direct arrival (black line) and first refraction (red line) in the 1 m spacing data but, as for Site 1, because these arrivals are observed on a small number of traces the determined intercept and velocity have relatively low accuracy. The second refraction can be defined with quite good accuracy. The 3 m spacing data show on a single arrival. The velocity of this arrival is similar to that of the second refraction in the 1 m data and it can be confidently interpreted as the same arrival. The velocity is most accurately defined by the 1 m spacing data The data from Site 2 contain no evidence of a frozen layer. All of the arrivals could be picked most accurately using reversed polarity responses.

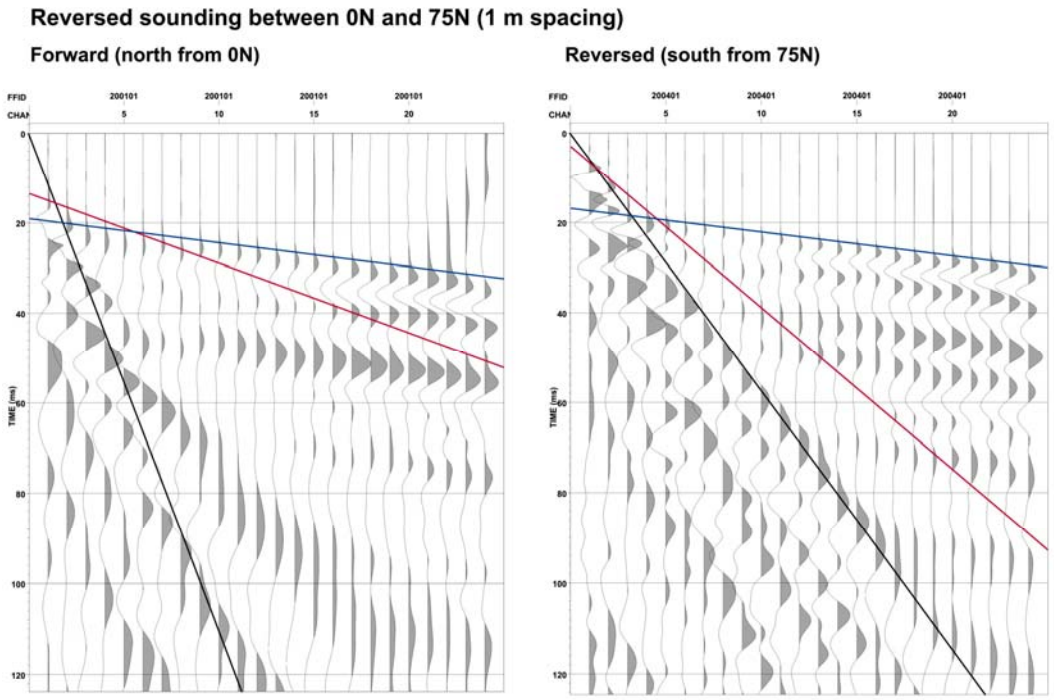

Figure 24: Seismic refraction profiles with 1 m geophone spacing from Site 2. Note that the results do not form a true reversed profile.

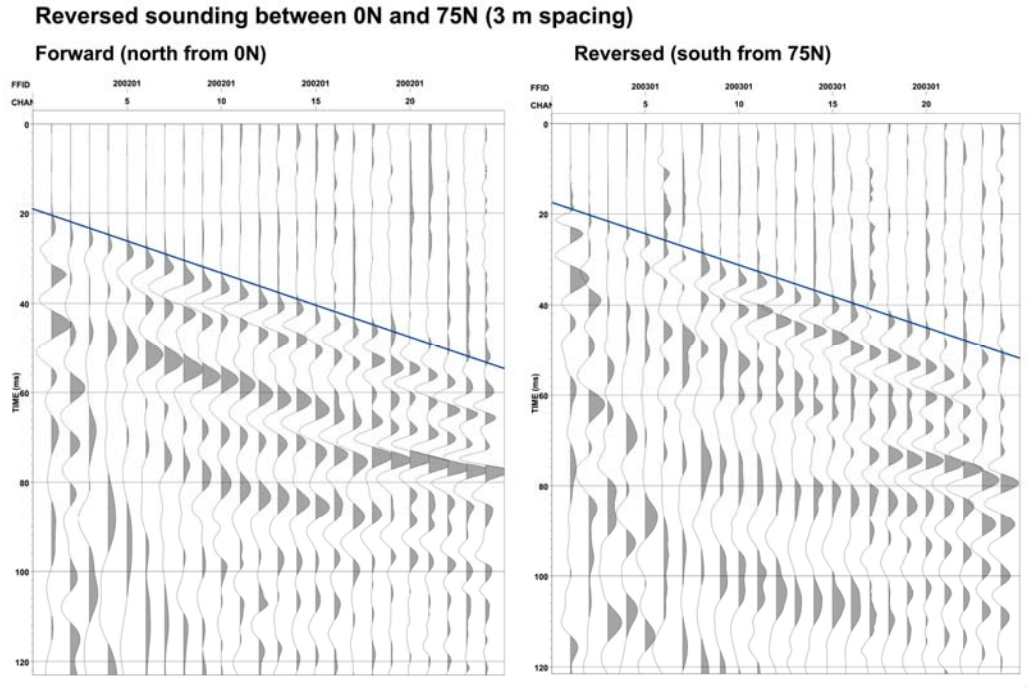

Figure 25: Seismic refraction profiles with 3 m geophone spacing from Site 2.

Table 4. Arrivals fitted to Site 2 seismic refraction data.

Arrival	Intercept (ms)	Velocity (m/s)	Arrival	Intercept (ms)	Velocity (m/s)
1 m spacing data					
Forward profile. Direction: north. File 200101			Reverse profile. Direction: south. File 200401		
1	0	89.93	1	0	174.2
2	13.78	633.0	2	3.33	269.8
3	19.02	1888.1	3	16.68	1903.0
3 m spacing data					
Forward profile. Direction: north.	File 200201		Reverse profile. Direction: south. File 100301		
3	19.03	2084.7	3	17.53	2174.7

Table 5 lists the seismic model fitted to each of the shots from Site 2 using theory appropriate for a locally horizontally-layered medium. The parameters of the arrivals were determined from the 1 m geophone spacing data. The data has sufficient resolution to indicate the presence of two near-surface layers and the fact that these layers may be different between either end of the profile. However, the specific parameters of the layers are poorly determined. The two parameters that are quite well determined by the data are the depth to the third layer which is approximately 2.1±0.2 m and the velocity of the third layer, which is 1900±100 $m.s^{-1}$.

Table 5. Arrivals fitted to Site 2 seismic refraction data.

Layer	Velocity (m/s)	Thickness (m)	Layer	Velocity (m/s)	Thickness (m)
1 m spacing data					
Forward profile. End: south. File 200101			Reverse profile. End: north. File 200401		
1	89.93	0.63	1	174.2	0.38
2	633.0	1.72	2	269.8	2.35
3	1888.1		4	1903.0	

5.2 Integrated data analysis and interpretation

5.2.1 Near-surface structure

The terrain conductivity data from Site 2 indicate the presence of a laterally varying conductivity structure and a general increase in conductivity with depth. The EM38 horizontal dipole mode response shows significant lateral variations suggesting that a component of the conductivity variations must be occurring within the upper 1 m at the site. The north end of the seismic refraction data is relatively close to the south end of the terrain conductivity grid and shows lower interfaces at 38 cm and around 3 m depth. The EM results suggest that conductivity variations are occurring in the second layer. The seismic velocity of this layer was significantly higher, and the layer is thicker, at the north end of the profile near the apparent conductivity high, than at the south end. Taken together, the seismic and EM results are consistent with an increase in the thickness and clay content of the second layer causing the conductivity high.

Gowan & Ferguson (2005) describe the analysis of a more extensive data set from Site 2. Their analysis identifies the northwest-southeast trending conductivity feature and show that this feature forms a localized anomaly in a more resistive background. In the previous study DC-

resistivity and terrain conductivity data were modelled and interpreted to provide the shallow structure shown in Table 6. The conductive feature is interpreted to be caused by variation in a sand/silt layer between around 15 cm and 1.5 m depth.

Table 6. Shallow conductivity structure and interpretation at Site 2 from Gowan & Ferguson (2005).

Layer	Background Area		Conductive Area		Interpretation
	Depth to Base (m)	Conductivity ($mS.m^{-1}$)	Depth to Base (m)	Conductivity ($mS.m^{-1}$)	
1	0.2	10	0.1	60	Soil
2	1.6	5	0.9	14	Fine-grained sand/silt
3	2.8	200	2.1	200	Silt/clay
4	35	7		6	Sand gravel

The results of the present survey are reasonably consistent with those in Gowan & Ferguson (2005). The seismic refraction data from the present study were collected with a multi-channel instrument and are likely superior to those from the single-channel instrument in the previous study. The present data set suggests that the base of the second layer is at 2 to 3 m depth which is deeper than determined in the earlier study (and also requiring the depth determined for the base of the third layer to be greater). The velocity determined for the third layer is in reasonable agreement between the two studies. The relatively high velocity and high conductivity determined in DC-resistivity studies (Gowan & Ferguson 2005) allows the layer to be interpreted as clay-rich basinal deposits. The results from the present study suggest that the conductivity anomaly is caused by a variation in the lithology of the second layer rather than a localized ridge in the conductive third layer as suggested in Gowan & Ferguson (2005).

5.3 Conclusions

Two geophysical surveys were completed at Site 2 in 2007, terrain conductivity and seismic refraction surveys. The terrain conductivity results defined a linear northeast-southwest trending conductivity high that had been detected in previous surveys at the site. The conductivity high is interpreted to be caused by an increase in the clay content of a layer which, based on previous findings and current seismic refraction interpretations, extends from around 15 cm to around 2-3 m depth. This layer overlies a layer with relatively high velocity and conductivity that is interpreted to be clay-rich basinal deposits.

Acknowledgements

The 2007 Geophysics Field School students collected the geophysical data presented in this report on April 24th, and 26th 2007 and additional data was collected by J. McCutcheon and T. Unrau on May 18th. The 2007 Field School consisted of: students D. Toni, L. Rosenthal, P. Bucher, L. Stewart, D. Card, I. Kurosawa, K. Olaleye, T. Unrau, L. Groshak, S. Idowu, H. Sealey, and K. van Dronglen; Teaching Assistant A. Krakowka; and instructors M. Serzu, I. Ferguson and A. Frederiksen. Manitoba Conservation is thanked for granting access to the park for field school training. We also thank the Natural Sciences and Engineering Research Council of Canada (NSERC) for providing Undergraduate Research Awards to T.U. and C.T. through which this work was completed.

References

Bison Instruments, 1975. Instruction manual, Bison Instruments earth resistivity meters. Bison Instruments Incorporated, Minneapolis, Minnesota, 24 p.

Geonics, 1991. EM31 operating manual. Geonics Limited, Mississauga, Ontario, 61 p.

Gowan, E. J. & Fergusson, I.J., 2005. Geophysical Survey of the Birds Hill Esker Complex at Birds Hill Provincial Park, Manitoba. University of Manitoba, 46p.

Matile, G., 1984. Quaternary geology map of the Birds Hill area. Manitoba Energy and Mines, Mines Division, Map AR84-5, scale 1:20 000.

Reynolds, J.M., 1997. An Introduction to Applied and Environmental Geophysics. John Wiley & Sons Ltd. West Sussex, England, 796 p.

Sandberg, S.K., 2005. Inverse modeling software for resistivity, induced polarization (IP), and transient electromagnetic (TEM, TDEM) soundings. Instruction Manual for EINVRT6, Geophysical Solutions, Albuquerque, New Mexico, U.S. , 39 p.

Sandberg, S. K., 1988, Microcomputer software for the processing and forward modeling of transient electromagnetic data taken in the central loop sounding configuration: New Jersey Geological Survey Open-File Report 88-1, 88p., 1 diskette.

Scott, W.J., Sellmann, P.V, and Hunter, J.A, 1990, Geophysics in the study of permafrost. In Geotechnical and Environmental Geophysics, Vol 1. Ed. S.H.Ward, SEG.

Telford, W. M., Geldart, L. P., & Sheriff, R. E. 1990. Applied Geophysics, Cambridge University Press, Cambridge, 2nd edition, 770 p.